Chapter 7

Thermal fluctuations in pattern-forming instabilities

Statistics is the physics of numbers.

P. Diaconis

Thermal fluctuations result from deterministic chaos in 10^{23} dimensions.

I. Rehberg

The material in this chapter has been published as Ref. [114]. Landau's method of hydrodynamic fluctuations is developed in a form suitable for pattern-forming systems. The resulting scheme is applied to RBC, to Taylor-Couette flow and to the SM of EHC. Using the WEM would lead to a factor of two (two critical left- and right travelling modes instead of one stationary mode) that is cancelled by the correlation time in the denominator of Eq. (7.41), which the WEM predicts to be twice as long as in the SM (Chapter 6.4).

7.1 Introduction

Recent experiments in several hydrodynamic systems confirm that pattern-forming instabilities in extended nonequilibrium systems exhibit some features reminiscent of equilibrium-phase transitions. Fluctuations of the field variables become measurable near threshold and both their amplitudes and the correlations in space and time increase as one approaches the threshold. Two questions arise. Are the measured fluctuations of internal origin, i.e., due to thermal or quantum-mechanical noise (the latter is predominant in lasers [115]) or are they the result of external noise from the experimental setup? Can one theoretically describe thermal fluctuations in pattern-forming systems in an unified way, as in equilibrium systems? A positive answer

to the second question means extending the theory of fluctuations near equilibrium phase transitions [68] to nonequilibrium systems. If in addition the predictions are confirmed by experiments as discussed in the Sections 5 and 6 of this chapter, it is safe to say that one actually measured thermal fluctuations. Each additional source would increase the fluctuations.

Theoretical predictions for the effects of thermal noise in pattern-forming systems were given for Rayleigh–Bénard convection (RBC) in simple fluids [116, 117, 118] and recently for RBC in binary mixtures [119], for electrohydrodynamic convection (EHC) in nematic liquid crystals (NLC) [120] and for Taylor–Couette flow (TCF) [121, 122, 123]. In all this work, the dynamical (macroscopic) equations are suppplemented with stochastic terms accounting for the microscopic degrees of freedom and determined from the assumption of local equilibrium. Near threshold the resulting Langevin equations are reduced to a stochastic generalization of the usual normal form equations. These equations are simple enough to be solved for the amplitude (and phase) fluctuations and may provide a basis for an unified description of fluctuations of patterns in nonequilibrium systems. Once the amplitude fluctuations are known the determination of the fluctuations of the physical fields and their measurable effects is straightforward.

The crucial assumption in this approach is that of local equilibrium in systems which are typically far from global equilibrium. This implies that the external forces driving the system out of equilibrium, e.g., shear, director rotation, electric and magnetic fields, and also the ensuing fields of the macroscopic patterns, are small compared to the internal fields effective on a molecular scale. In the hydrodynamic regime this should be always fulfilled.

In the next two sections I describe the method in a form applicable to a large class of pattern-forming systems including quasi one-dimensional (1D) and quasi two-dimensional (2D) systems and the interesting case of symmetry-induced degeneracy where several deterministic solutions become simultaneously unstable at the primary threshold. In Section 4 I calculate the fluctuations of planar EHC and compare them with fluctuations of RBC patterns in simple liquids and axisymmetric vortices in TCF. Chapter 7.5 describes relevant experiments which are compared to the theory in the last section.

7.2 Macroscopic stochastic equations for thermal noise

With the assumption of local equilibrium one can use locally the fluctuation-dissipation theorem (FDT) which essentially states that thermal fluctuations are always connected with dissipation and vice versa. So I start by writing down the ensemble-averaged entropy production of the macroscopic system as an integrated sum of products of

Onsager forces and currents (summation over doubly occurring indices is implied)

$$\langle \dot{S} \rangle = \int_V d^3\boldsymbol{r} \left\{ F_\alpha(\boldsymbol{r},t) \langle J_\alpha(\boldsymbol{r},t) \rangle \right\} . \tag{7.1}$$

For macroscopic hydrodynamic systems near local equilibrium this quantity is extensive and the forces and ensemble-averaged currents, F_α and $\langle J_\alpha \rangle$, are linearly related,

$$\langle J_\alpha \rangle = M_{\alpha\beta} F_\beta := J_\alpha - \tilde{J}_\alpha , \tag{7.2}$$

where $M_{\alpha\beta}$ are the components of the Onsager matrix $\underline{\underline{M}}$, given by the constitutive material equations. We allow for fluctuations $\tilde{J}_\alpha$ of the currents, $J_\alpha = \langle J_\alpha \rangle + \tilde{J}_\alpha$ with $\langle \tilde{J}_\alpha \rangle = 0$, and will determine them with the FDT. Introducing auxiliary field variables $x_\alpha(\boldsymbol{r},t)$ by $J_\alpha = \dot{x}_\alpha$ (Ref. [68]) one can write the constitutive relations (7.2) with fluctuations as Langevin equation for x_α,

$$\dot{x}_\alpha = M_{\alpha\beta} F_\beta + \tilde{J}_\alpha . \tag{7.3}$$

Expressing the entropy $S[\boldsymbol{x}] = \int_V d^3\boldsymbol{r}\, s(\boldsymbol{x}(\boldsymbol{r}))$ in terms of $\boldsymbol{x}$ ($\boldsymbol{x}$ is a shorthand for all x_α) and comparing the averaged entropy production $\langle \dot{S}\,[\boldsymbol{x}] \rangle = \int_V d^3\boldsymbol{r} \frac{\partial S}{\partial x_\alpha} \langle \dot{x_\alpha} \rangle$ with (7.1), one sees that the forces are the variables conjugate to x_α, $F_\alpha = \frac{\partial S}{\partial x_\alpha}$, and (7.3) can be written in a "generalized potential form" $\dot{x}_\alpha = M_{\alpha\beta} \frac{\partial S}{\partial x_\beta} + \tilde{J}_\alpha$. For a given small volume element ΔV_r around $\boldsymbol{r}$, the corresponding Fokker-Planck equation allows a canonical stationary distribution $W_{\infty,r}[\boldsymbol{x}] \propto e^{S_r/k_B}$ with $S_r = \int_{\Delta V_r} d^3\boldsymbol{r}\, s(\boldsymbol{x}(\boldsymbol{r})) \approx s \Delta V_r$, if the probability currents are zero (detailed balance) and the fluctuations are given by the fluctuation-dissipation theorem $\langle \tilde{J}_\alpha(\boldsymbol{r},t) \tilde{J}_\beta(\boldsymbol{r}',t') \rangle = k_B (M_{\alpha\beta} + M_{\beta\alpha}) (\Delta V_r)^{-1} \delta_{rr'} \delta(t-t')$ [68, 124]. In the continuum limit this becomes

$$\langle \tilde{J}_\alpha(\boldsymbol{r},t) \tilde{J}_\beta(\boldsymbol{r}',t') \rangle = k_B (M_{\alpha\beta} + M_{\beta\alpha}) \delta(\boldsymbol{r}-\boldsymbol{r}') \delta(t-t') . \tag{7.4}$$

Thus the FDT is a consequence of the postulated canonical distribution. Note that this ansatz implies the existence of "mesoscopic" volume elements which are large enough so that the entropy can be treated as extensive quantity and small enough to neglect spatial variations of the macroscopic fields.

Typical sources contributing to the density $\dot{s}$ of the entropy production (7.1) are $\dot{s}^{(v)}$ related to the viscous flow and $\dot{s}^{(th)}$ related to thermal conductivity. In fluids with finite electric conductivity there is a contribution $\dot{s}^{(el)}$ due to Ohmic heating, and in NLCs an additional contribution $\dot{s}^{(n)}$ from the orientational relaxation of the director field $\boldsymbol{n}(\boldsymbol{r},t)$ [72]. These sources are [120, 58, 125]

$$\begin{aligned} T\,\dot{s}^{(v)} &= \sigma^{(s)}_{ij} v_{ij}, & T\,\dot{s}^{(n)} &= -\sigma^{(as)}_{ij} \Omega_{ij}, \\ T\,\dot{s}^{(th)} &= -\tfrac{1}{T} \boldsymbol{j}^{(th)} \cdot \boldsymbol{\nabla} T, & T\,\dot{s}^{(el)} &= \boldsymbol{j}^{(el)} \cdot \boldsymbol{E}, \end{aligned} \tag{7.5}$$

where $v_{ij} = (\partial_i v_j + \partial_j v_i)/2$ is the symmetrical fluid shear-rate tensor $n_j \Omega_{ij} = n_j(\partial_i v_j - \partial_j v_i)/2 + (\partial_t + \boldsymbol{v} \cdot \boldsymbol{\nabla}) n_i$ is the rotation of the director relative to the moving fluid, $\sigma_{ij}^{(s)}, \sigma_{ij}^{(as)}$ are the symmetric and antisymmetric parts of the stress tensor and $\boldsymbol{j}^{(th)}$ and $\boldsymbol{j}^{(el)}$ are the dissipative parts of the heat and electric current. This list is not complete; for example in binary mixtures there is an additional mixing-entropy term proportional to the negative concentration gradient times the mass flux density of one component, see e.g., [119, 126, 58].

There is some freedom in choosing the Onsager forces and currents. If one takes as currents

$$\{J_\alpha\} = (\sigma_{ij}^{(s)}, \quad \sigma_{ij}^{(as)}, \quad j_i^{(th)}, \quad j_i^{(el)}) \tag{7.6}$$

then the conjugate forces are

$$\{F_\alpha\} = \left(\frac{v_{ij}}{T}, \quad -\frac{\Omega_{ij}}{T}, \quad -\frac{\partial_i T}{T^2}, \quad \frac{E_i}{T} \right), \tag{7.7}$$

and the Onsager matrices can be found by comparing the dissipative part of the constitutive material equations with the definitions of the currents and forces.

For NLCs the constitutive equations are (Chapter 2 and [57, 58])

$$\begin{pmatrix} \sigma_{ij}^{(s)} \\ \sigma_{ij}^{(as)} \\ j_i^{(th)} \\ j_i^{(el)} \end{pmatrix} = \begin{pmatrix} T\eta_{ij,kl} & T\eta_{ij,kl}^{(n)} & 0 & 0 \\ T\eta_{kl,ij}^{(n)} & T\gamma_{ij,kl} & 0 & 0 \\ 0 & 0 & T^2\lambda_{ik} & -T\lambda_{ik}^{(el)} \\ 0 & 0 & -T\lambda_{ik}^{(el)} & T\sigma_{ik}^{(el)} \end{pmatrix} \begin{pmatrix} v_{kl}/T \\ -\Omega_{kl}/T \\ -\partial_k T/T^2 \\ E_k/T \end{pmatrix}, \tag{7.8}$$

with the NLC-Onsager matrix as first term on the right-hand side. The viscosity tensor $\eta_{ij,kl}$, the rotational viscosity tensor $\gamma_{ij,kl}$ and the fluid-director coupling $\eta_{ij,kl}^{(n)}$ contain a total of five independent coefficients (for $\eta_{ij,kl}$ see Eq. (2.20), for the other tensors see Eq. (B1) in [120]). The thermal and electric conductivities λ_{ik} and $\sigma_{ik}^{(el)}$ and the Peltier coefficients $\lambda_{ik}^{(el)}$ are uniaxial tensors of the form $\lambda_\perp \delta_{ik} + \lambda_a n_i n_k$.

To get the noise terms of the macroscopic equations themselves, one identifies all parts which may contain dissipative effects and writes them in terms of the Onsager currents. Typically these equations, written in terms of the perturbations $\boldsymbol{u}(\boldsymbol{r}, t)$ of the macroscopic fields from the unstructured state, can be cast into the symbolic form (the field variables $\boldsymbol{u}$ should not be confused with the auxiliary variables $\boldsymbol{x}$ in the derivation of the FDT),

$$[\underline{\underline{S}}^R(\boldsymbol{\nabla}, \boldsymbol{r}, t)\partial_t + \underline{\underline{L}}^R(\boldsymbol{\nabla}, \boldsymbol{r}, t)]\boldsymbol{u}(\boldsymbol{r}, t) + \boldsymbol{N}^R(\boldsymbol{u}, \boldsymbol{\nabla}, \boldsymbol{r}, t) = \boldsymbol{\xi}(\boldsymbol{r}, t), \tag{7.9}$$

with the noise term $\boldsymbol{\xi}$ to be determined. The linear matrix-differential operators $\underline{\underline{S}}^R$ and $\underline{\underline{L}}^R$ and the nonlinear deterministic term $\boldsymbol{N}$ depend on a control parameter R and may depend explicitely on $\boldsymbol{r}$ if the basic state is nontrivial (e.g., in TCF or

Non–Boussinesq RBC) or periodically on time in the case of periodic forcing as in EHC. Recall from chapter 2 that the mascroscopic equations are either conservation laws or balance equations for slowly relaxing variables or broken-symmetry variables; the latter are e.g., director variations in NLC. The first class of equations contains gradients of the currents (examples 1 and 2 below), the second one some linear combination of the currents themselves. In both cases, the left-hand side of Eq. (7.9) can be written symbolically as

$$(\underline{\underline{S}}^R\partial_t + \underline{\underline{L}}^R)\boldsymbol{u} \equiv -\underline{\underline{D}}\langle \boldsymbol{J}\rangle + \text{conservative terms}, \tag{7.10}$$

where $\boldsymbol{J}$ contains all Onsager currents and $\underline{\underline{D}}$ is a matrix-differential operator for conservation laws and a matrix for other balance equations. The stochastic forces are accordingly

$$\boldsymbol{\xi}(\boldsymbol{r},t) = \underline{\underline{D}}\tilde{\boldsymbol{J}}(\boldsymbol{r},t). \tag{7.11}$$

In summary, the Langevin equations (7.9) are a stochastic generalization of the deterministic basic equations. The fluctuating forces $\boldsymbol{\xi}$ have zero mean and their second moments are given in terms of $\underline{\underline{D}}$ and the Onsager matrix $\underline{\underline{M}}$ by (7.11) and (7.4). $\underline{\underline{M}}$ is defined *via* the constitutive material equations (Eqs. (7.8) for NLCs)) and $\underline{\underline{D}}$ by the basic equations themselves (see examples below). Note that $\underline{\underline{M}}$ and $\underline{\underline{D}}$ may depend on broken-symmetry variables and in addition $\underline{\underline{M}}$ on scalar fields (temperature etc.) of the basic equations, giving rise to multiplicative parts of $\boldsymbol{\xi}$ in terms of the macroscopic field variables. As an example, the constitutive NLC material tensors depend on the director $\boldsymbol{n}$, which is also a macroscopic variable in the EHC equations.

Now I give some examples for $\underline{\underline{D}}$.

1. Navier-Stokes equations for an incompressible fluid, $\rho_m(\partial_t + \boldsymbol{v}\cdot\boldsymbol{\nabla})\boldsymbol{v} + \boldsymbol{\nabla}p - \boldsymbol{\nabla}\langle\underline{\underline{\sigma}}\rangle - \boldsymbol{f}_{vol} = \boldsymbol{\xi}^{(v)}$. All dissipative effects are contained in $\boldsymbol{\nabla}\underline{\underline{\sigma}}$, which can be written (in Cartesian coordinates) as $(\boldsymbol{\nabla}\underline{\underline{\sigma}})_i = \partial_j(\sigma_{ji}^{(s)} + \sigma_{ji}^{(as)}) = D_{i,jk}(\sigma_{jk}^{(s)} + \sigma_{jk}^{(as)})$ with $D_{i,jk} = \delta_{ik}\partial_j$. Hence $\xi_i^{(v)} = D_{i,jk}(\tilde{\sigma}_{jk}^{(s)} + \tilde{\sigma}_{jk}^{(as)})$.

2. Heat equation (conservation of energy) $\rho_m c_v(\partial_t + \boldsymbol{v}\cdot\boldsymbol{\nabla})T + \boldsymbol{\nabla}\cdot\langle\boldsymbol{j}^{(th)}\rangle = \xi^{(th)}$. Obviously $\underline{\underline{D}} = -\boldsymbol{\nabla}$ and $\xi^{(th)} = -\boldsymbol{\nabla}\cdot\tilde{\boldsymbol{j}}^{(th)}$. Things are analogous for the charge conservation equation.

3. Director equations in EHC (balance of local angular momentum), $\boldsymbol{n}\times\boldsymbol{\Gamma} = \boldsymbol{\xi}^{(n)}$, where $\boldsymbol{\Gamma}$ is the molecular field introduced by De Gennes [25]. Here the dissipative terms are not so obvious. They are proportional to the antisymmetric part of the stress tensor, $(\boldsymbol{n}\times\boldsymbol{\Gamma})_i = (\boldsymbol{n}\times\boldsymbol{\Gamma})_i^{(cons)} + \epsilon_{ijk}\langle\sigma_{jk}^{(as)}\rangle$, i.e., $\xi_i^{(n)} = -\epsilon_{ijk}\tilde{\sigma}_{jk}^{(as)}$ [72, 120, 127], where ϵ_{ijk} is the total-antisymmetric third-rank unity tensor.

7.3 Stochastic amplitude equations

Amplitude equations (normal forms), valid near threshold in systems with a continous bifurcation, are universal in a way that they only depend on the symmetries of the pattern and on the quasi-dimensionality of the system. *Stochastic* amplitude equations seem a natural way to generalize this universality to fluctuations of patterns, and compare them to equilibrium fluctuations near continous phase transitions. We define as quasi-dimensionality D the number of dimensions (0, 1 or 2) where the system is translationally invariant and infinite. Of course "infinite" means sufficiently large so that boundaries play no role; for stationary patterns this means a system size much larger than the correlation length of the pattern; for travelling waves the precise conditions are not yet well understood, but seem to be more stringent [9]. Denoting the infinite directions with $r_\parallel$ and the other "perpendicular" directions with $r_\perp$, a space point is given for $D = 2$ by $\boldsymbol{r} = (r_{\parallel 1}, r_{\parallel 2}, r_{\perp 1})$ and for $D = 1$ by $\boldsymbol{r} = (r_{\parallel 1}, r_{\perp 1}, r_{\perp 2})$. The $r_\perp$-coordinates are allowed to be curvilinear. We will use vector notation for $r_\parallel, r_\perp$ only if they explicitely have more than one component.

The symmetries of the correlations of the fluctuating pattern below threshold are determined by the branches of the linear deterministic growth rate $\lambda(\epsilon, k) = \mathrm{Re}\lambda(\epsilon, k) - i\omega(\epsilon, k)$ for the modes $\boldsymbol{u}_k = e^{\lambda t} e^{ik \cdot r_\parallel}\, \boldsymbol{f}^R(k, r_\perp, t)$ becoming first unstable at threshold, where $\boldsymbol{f}^R$ is periodic in t in systems with periodic driving like AC-driven EHC. The reduced control parameter $\epsilon = (R - R_c)/R_c$ and the threshold, $\lambda(\epsilon = 0, k_c) = -i\omega_c$, are defined as usual. A bifurcation is stationary if $\omega_c = 0$, and degenerate if the growth rate of the critical branch becomes simultaneously unstable around several k_c values or if there are several critical dispersion branches, e.g., associated with a Hopf bifurcation $\lambda(\epsilon = 0, k_c) = \pm i\omega_c$.

The amplitude equations are usually derived by a multiple-scale perturbation around threshold [9, 10], but for the linear part the resulting solvability conditions determining the amplitude are equivalent to projecting the basic equations onto the critical eigenfunctions. We extend now this projection to the stochastic system and add, if necesary, the nonlinear deterministic terms *ad hoc*. The director-dependent parts of the fluctuating forces, described in the paragraph after Eq. (7.11), will lead to additional multiplicative noise terms also in the amplitude equation. Reference [120] gives plausibility arguments that within the range of validity of the amplitude equation they are negligible compared to the additive noise.

We show this projection for autonomous systems with non-degenerate bifurcations and make some remarks about more general cases later. Inserting the ansatz

$$\boldsymbol{u}(\boldsymbol{r}, t) = \int d^D k' e^{i(k' \cdot r_\parallel - \omega t)} \psi(k', t) \boldsymbol{f}^R(k', r_\perp) \tag{7.12}$$

in the linear part of (7.9) and projecting these equations onto the eigenfunctions of

the adjoint linear problem gives a stochastic linear equation for the mode amplitudes,

$$\partial_t \psi(k,t) = \lambda(\epsilon,k)\psi(k,t) + \Gamma(k,t). \tag{7.13}$$

The noise term is

$$\Gamma(k,t) = \frac{[\boldsymbol{f}^{\dagger R}, \boldsymbol{\xi}(t)]}{[\boldsymbol{f}^{\dagger R}, \underline{\underline{S}}^R(\nabla_\parallel \to ik, \nabla_\perp, r_\perp)\boldsymbol{f}^R]}, \tag{7.14}$$

where $\nabla_\parallel$ and $\nabla_\perp$ are the components of the nabla operator in the $r_\parallel$ and $r_\perp$ directions, respectively. The brackets denote the scalar product

$$[\boldsymbol{\phi}, \boldsymbol{\eta}] := \frac{1}{C}\int_C d^{3-D} r_\perp \phi^*_\alpha(r_\perp)\eta_\alpha(r_\perp), \tag{7.15}$$

for vector functions $\boldsymbol{\phi}$ and $\boldsymbol{\eta}$ containing fields of the basic equations and defined in C where C is the cross-section for $D = 1$ and the thickness for $D = 2$. The Hermitean conjugate operators in the adjoint linear problem $(\underline{\underline{S}}^{R\dagger}\partial_t + \underline{\underline{L}}^{R\dagger})e^{-i(k\cdot r_\parallel - \omega t)}\boldsymbol{f}^{\dagger R}(k, r_\perp) = 0$ are defined with respect to this scalar product.

Inserting (7.11) and (7.4) into (7.14) gives $\langle\Gamma\rangle = \langle\Gamma\Gamma\rangle = \langle\Gamma^*\Gamma^*\rangle = 0$ and the noise strength [120]

$$\langle\Gamma^*(k,t)\Gamma(k',t')\rangle = Q^R(k)(2\pi)^{-D}\delta(k-k')\delta(t-t'), \tag{7.16}$$

$$Q^R(k) = \frac{1}{C}\frac{[\boldsymbol{f}^{\dagger R}, \underline{\underline{Q}}(ik, \nabla_\perp, r_\perp)\boldsymbol{f}^{\dagger R}]}{|[\boldsymbol{f}^{\dagger R}, \underline{\underline{S}}^R(ik, \nabla_\perp, r_\perp)\boldsymbol{f}^R]|^2}. \tag{7.17}$$

The noise-correlation matrix of the basic equations, defined (in real space) as $\langle\boldsymbol{\xi}(\boldsymbol{r},t)\boldsymbol{\xi}(\boldsymbol{r}',t')\rangle = \underline{\underline{Q}}(\boldsymbol{\nabla}, \boldsymbol{r})\delta(\boldsymbol{r}-\boldsymbol{r}')\delta(t-t')$, is given by

$$\underline{\underline{Q}}(\boldsymbol{\nabla}, r_\perp) = k_B \underline{\underline{D}}(\underline{\underline{M}} + \underline{\underline{M}}^T)\underline{\underline{D}}^\dagger. \tag{7.18}$$

where $\underline{\underline{D}}^\dagger$ is the Hermitean conjugate of $\underline{\underline{D}}$ with respect to the scalar product (7.15). The intensity of stationary fluctuations of the modal amplitudes resulting from Equation (7.13) with (7.16) is

$$\langle|\psi(k)|^2\rangle = \frac{Q^R(k)}{2(2\pi)^D \mathrm{Re}(-\lambda)}. \tag{7.19}$$

The above eqations are valid in the linear regime and in particular for any k and $\epsilon \le \epsilon_{NL} < 0$ (for all practical purposes $\epsilon_{NL} \approx 0$, see [118]). Now I specialize to the vicinity of the threshold and consider only contributions near $\pm k_c$ since the stationary mode fluctuations (7.19) are large only in these regions. Expanding the linear modal growth rate $\lambda(\epsilon, k)$ to lowest nontrivial order around threshold and evaluating the

stochastic terms at threshold one obtains from (7.13) the main result of this section, the amplitude equation in real space,

$$\begin{aligned} \tau_0(\partial_t + v_g \cdot \nabla_\parallel)A(r_\parallel,t) &= (\epsilon + \xi_{ij}\nabla_{\parallel i}\nabla_{\parallel j})A(r_\parallel,t) \\ &+ \tau_0\sqrt{Q}\ \eta(r_\parallel,t), \qquad (7.20) \\ Q &= Q^{R_c}(k_c). \qquad (7.21) \end{aligned}$$

The amplitude $A(r_\parallel,t)$ is defined by its Fourier tansform, $A(q,t) = \psi(k_c+q,t)$. The deterministic coefficients $\tau_0^{-1} = \partial_\epsilon\lambda$, $v_g = \nabla_k\omega$ and $\xi_{ij} = -\frac{\tau_0}{2}\partial_{k_i}\partial_{k_j}\lambda$ (τ_0, ξ_{ij} in general complex) come from the expansion of $\lambda(\epsilon, k_c - i\nabla_\parallel) + i\omega_c$ to lowest nontrivial order around threshold and $\eta(r_\parallel,t)$ is a complex Gaussian noise source with $\langle\eta\eta\rangle = \langle\eta^*\eta^*\rangle = 0$ and $<\eta^*(r_\parallel,t)\ \ \eta(r'_\parallel,t')>= \delta(r_\parallel - r'_\parallel)\delta(t-t')$.

An example of the resulting equal-time correlations $<A^*(r_\parallel + \Delta r_\parallel, t)A(r_\parallel,t)>$- $= \int d^D r_\parallel e^{iq\Delta r_\parallel} Q/(2(2\pi)^D \mathrm{Re}\lambda)$ for 1D with $r_\parallel = x$ and real coefficients is

$$\langle A^*(x+\Delta x,t)A(x,t)\rangle = \frac{Q\tau_0 e^{-\left|\frac{\Delta x\sqrt{-\epsilon}}{\xi_0}\right|}}{8\xi_0\sqrt{-\epsilon}}. \qquad (7.22)$$

Since (7.20) is an inhomogeneous equation, the precise connection with the physical quantities is essential. We get from (7.12) near threshold

$$\boldsymbol{u}(\boldsymbol{r},t) = A(r_\parallel,t)\boldsymbol{f}(r_\perp)e^{i(k_c\cdot r_\parallel - \omega_c t)} + \text{c.c.} + \text{h.o.t.} \qquad (7.23)$$

Now I discuss some generalizations.

For discretely degenerated bifurcations, e.g., zig and zag rolls $(\omega_c, k_{cx}, k_{cy}) = (0, k_{cx}, \pm k_{cy})$ in EHC in the oblique-roll regime[48], left and right travelling waves $(\pm\omega_c, k_{cx}, 0)$ in EHC in thin and clean cells [97] or in 1D-RBC in binary mixtures and other sytems, or both degeneracies [30], there are amplitude equations of the form (7.20) for each set $\pm k_c$ of modes around the critical k vectors. They are independent in the linear regime if the different (ω_c, k_c) values are sufficiently separated.

For isotropic systems e.g., RBC in isotropic fluids, EHC or RBC in homeotropically aligned EHC (see e.g., [23]) or optical vortices in large-aperture class A lasers [128] λ is of the form $\lambda = \lambda(\boldsymbol{k}^2, \epsilon)$. Inverse Fourier transform of (7.13) and substituting for the growth rate a generic isotropic expression approximating λ near threshold to $\mathcal{O}(k^2 - k_c^2)^2$ and $\mathcal{O}(\epsilon)$, gives with the same approximations as above the stochastic Swift-Hohenberg (SSH) equation

$$\tau_0\partial_t\psi(\boldsymbol{r}_\parallel,t) = \left(\epsilon - \tilde{\xi}_0^4(k_c^2 + \nabla_\parallel^2)^2\right)\psi + \tau_0\sqrt{Q}\eta(\boldsymbol{r}_\parallel,t), \qquad (7.24)$$

where $\tilde{\xi}_0^4 = -\frac{\tau_0}{2}\partial^2\lambda(k^2)/\partial(k^2)^2|_{k=k_c}$. The amplitude ψ, defined as the inverse spatial Fourier transform of $\psi(k,t)$, is related to the physical quantities in the case of stationary bifurcations by

$$\boldsymbol{u} = \psi(\boldsymbol{r}_\parallel,t)\boldsymbol{f}(r_\perp) + \text{h.o.t.} \qquad (7.25)$$

and its modes in k space have the fluctuation intensity (7.19). In contrast to the difficulties with the deterministic version of this equation in the weakly nonlinear regime (see e.g., [9]) it should be correct in describing subcritical fluctuations.

Nonautonomous systems with a periodic driving force like AC-driven EHC can be reduced (using the Floquet theorem and a discrete Fourier transformation in time) to an infinite set of autonomous equations for the components of $\boldsymbol{u}$ proportional to $e^{\pm in\omega_0 t}$, with the external driving frequency ω_0 and integer n [120]. Truncating at some $n = n_{max}$ gives an effectively autonomous system.

Note that expression (7.21) is valid for both the amplitude and the SSH equations and for any boundary conditions (BC) including lateral through flow. The actual value of Q changes because the eigenfunctions (and eventually $\underline{\underline{S}}$) depend on the BC and on the through flow. As shown in the next section, the fluctuations of the physical quantities, obtained from the amplitude fluctuations with (7.23) or (7.25), do not depend on the normalizations of $\boldsymbol{f}$ or $\boldsymbol{f}^\dagger$. They are, as equilibrium fluctuations calculated with the equipartition theorem, inversely proportional to the thickness (D=2) or to the cross section (D=1).

7.4 Theoretical results

At first I show how the method works by applying it to RBC in isotropic fluids, a pattern-forming system with one of the simplest basic equations. Then I calculate fluctuations of axisymmetric vortices in TCF, an example for an 1D system with curvilinear geometry and a nontrivial basic flow leading to an explicit $r_\perp$ dependence in the linearized basic equations. Finally I calculate the stochastic term of the anisotropic amplitude equation of quasi two-dimensional planar EHC. Here the basic equations are far more complex and depend (due to the periodic driving) explicitely on time. The calculations are rather lengthy but as straightforward as in the other systems.

7.4.1 Rayleigh–Bénard convection

We consider both a quasi two-dimensional system with a thickness d, $r_{||} = (x, y)$, $r_\perp = z$, and an 1D system with a rectangular cross-section $L_y d$, $r_\perp = (x, y)$ and $r_{||} = x$ where L_y and d are of the same order and so small that the unstable mode branch $\boldsymbol{f}^R(k, r_\perp)$ is well separated from the branches of other perpendicular modes. As order-parameter equations one can take for the 2D system the SSH equation (7.24) which has in this classical case real coefficients, and for the 1D system the amplitude equation (7.20), which specializes without through flow to

$$\tau_0 \partial_t A = (\epsilon + \xi_0^2 \partial_x^2) A + \tau_0 \sqrt{Q}\eta(r_{||}, t). \tag{7.26}$$

If the one-dimensional system has periodic BC in the y direction then τ_0 and Q are the same and ξ_0 is related to the SSH length $\tilde{\xi}_0$ by $\xi_0^2 = 4k_c^2\tilde{\xi}_0^4$. The coefficients can be written as integrals of the eigenfunctions over the cross section [9] and depend via the eigenfunctions on the BC. The basic equations (7.9) are the Navier-Stokes, heat balance and continuity equations for the deviations $(\boldsymbol{v}, \theta, p)$ of the velocity, temperature and pressure from the unstructured state $(\boldsymbol{v}_0, T, p_0)$ [9], where $\boldsymbol{v}_0 = 0$ without through flow.

The heat balance equation, written in terms of the temperature deviation, couples only to v_z and has the same stochastic term as in Example 2 in Section 2 above. By applying twice the curl operation on the Navier-Stokes equations and taking the z component an equation for v_z is obtained (see Eq (A.4) in [118]), which couples only to the temperature deviation and has the fluctuating force (compare with Example 1 in Section 2) $\xi_z = [\boldsymbol{\nabla} \times (\boldsymbol{\nabla} \times \boldsymbol{\xi}^{(v)})]_z = [\boldsymbol{\nabla} \times (\boldsymbol{\nabla} \times \boldsymbol{\nabla}\underline{\underline{\tilde{\sigma}}})]_z$.

We gather the ingredients $\underline{\underline{D}}, \underline{\underline{M}}$ and $\underline{\underline{D}}^\dagger$ of the noise-correlation matrix. For incompressible isotropic fluids the dissipative transport coefficients in (7.8) reduce to $\eta_{ij,kl} = \nu\rho_m(\delta_{ik}\delta_{jl} + \delta_{il}\delta_{jk})$, $\eta^{(n)}_{ij,kl} = 0$ and $\lambda_{ik} = c_v\rho_m\kappa\delta_{ik}$ where ν is the kinematic viscosity, κ the heat diffusion coefficient and c_v the specific heat per mass. The components of the Onsager matrix are $M^{(vv)}_{ij,kl} = T\nu\rho_m(\delta_{ik}\delta_{jl} + \delta_{il}\delta_{jk})$ for the velocity equations, $M^{(th,th)}_{ij} = c_v\rho_m T^2\kappa\delta_{ij}$ for the temperature balance, and zero for the mixed components. Writing ξ_z as $D^{(vv)}_{jk}\tilde{\sigma}_{jk}$ with $D^{(vv)}_{jk} = (\partial_z\partial_k - \delta_{3k}\boldsymbol{\nabla}^2)\partial_j = -D^{(vv)\dagger}_{jk}$ (all indices run from 1 to 3) and $D^{(th,th)} = -\boldsymbol{\nabla} = -\boldsymbol{D}^{(th,th)\dagger}$ from example 2 one gets $O^{(vv)} = -2k_BT\nu\rho_m(\partial_x^2 + \partial_y^2)\boldsymbol{\nabla}^4$, $O^{(th,th)} = -2k_BT^2\kappa c_v\rho_m\boldsymbol{\nabla}^2$, and zero for the two nondiagonal elements. To calculate the Hermitean conjugates I used the fact that $\boldsymbol{v}$ and θ vanish at the boundaries.

It is convenient to scale space by d, time by d^2/η and temperature by $P\Delta T/R$ with the Prandtl number $P = \eta/\kappa$ and the Rayleigh number $R = \Delta T g\alpha d^3/(\kappa\nu)$ where α is the heat expansion coefficient and $g = 9.81\mathrm{ms}^-2$. Choosing $\boldsymbol{k}_c = k_c\hat{\boldsymbol{x}}$ and inserting in (7.21) the noise-correlation matrix $\underline{\underline{Q}}$ and the time-derivative coefficients $S^{(vv)} = -\boldsymbol{\nabla}^2$, $S^{(th,th)} = P$ and $S^{(th,v)} = S^{(v,th)} = 0$ gives the noise intensity of both the nondimensionalized SSH and amplitude equations,

$$\begin{aligned} Q^{(R)} &= 2Q_0^{(R)} \\ &\times \frac{\int_{C'} d^{3-D}r_\perp \{f_z^{\dagger *}(k_c^2 - \partial_y^2)(k_c^2 - \nabla_\perp^2)^2 f_z^\dagger + \alpha^{(R)} f_\theta^{\dagger *}(k_c^2 - \nabla_\perp^2) f_\theta^\dagger\}}{|\int_{C'} d^{3-D}r_\perp \{f_z^{\dagger *}(k_c^2 - \nabla_\perp^2) f_z + P f_\theta^{\dagger *} f_\theta\}|^2}, \end{aligned} \tag{7.27}$$

with the (small) parameter

$$Q_0^{(R)} = \frac{k_BT}{\rho_m d\nu^2}. \tag{7.28}$$

The integrals go over the scaled cross section C' ($C' = 1$ for 2D, L_y/d for 1D and L_xL_y/d^2 for one Fourier mode) and f_z and f_θ denote the v_z and θ components of the eigenfunction at threshold. The relative contribution of the temperature fluctuations

turns out to be negligible for usual fluids [117, 118], but an analog will be essential in Taylor–Couette flow, so I will keep it.

If one multiplies equation (7.27) by a scalar product of any of the nonzero eigenfunction components f_z, f_x and f_θ (f_z and f_θ can be chosen real here and $iqf_x = -\partial_z f_z$) then the right-hand sides of the resulting equations are manifestly independent of the normalizations. Furthermore some scalar products relate the resulting equations directly to measurable effects of the fluctuations as can be seen from the left-hand sides of the following examples with (7.25) or (7.23) and $\langle\psi^*\psi\rangle$ (or $\langle A^*A\rangle$) $\propto Q$. Multiplying equation (7.27) with $([f_z,f_z]+[f_x,f_x])\rho_m C'/2$ makes its sides proportional to $\rho_m/2\int d^{3-D}r_\perp\langle v^2\rangle$, the mean energy per length (2D) or per area (1D), contained in the velocity fluctuations (see below). Multiplying both sides with $C'[f_\theta,f_\theta]$ relates them to the cross-section integrated temperature fluctuations proportional to the shadowgraph signal as discussed in Section 5. The simplest expression is obtained by multiplying (7.27) with $[f_z,f_\theta]$, relating the sides to the relative increase $N-1 = R_c^{-1}[f_z,f_\theta]\langle|\psi|^2\rangle$ of the heat transport due to convection (N is the Nusselt number) which is again a (globally) measurable quantity. This gives

$$[f_z,f_\theta]Q^{(R)} = \frac{2Q_0^{(R)}(1+\alpha^{(R)})}{C'\tau_0^{2(R)}}. \tag{7.29}$$

For 2D and free-slip BC (or 1D with additional periodic BC at $\pm L_y/2$ and $\partial_y = 0$), one has $\tau_0 = 2(P+1)/(3\pi^2)$ and Eq. (7.29) is (after taking care of the different scalings and relations to the physical variables) the classic result of Graham [117, 129]. For no-slip BC $\tau_0 = (P+0.512)/19.65$ [118] and (7.29) is the result of van Beijeren and Cohen [130]. The BC and the dimensionality enter *via* τ_0 and the projection integral. In particular, cross-section integrated fluctuating quantities rather than the fluctuations themselves are independent of the transverse system size.

As an example I give for the 1D system with periodic BC and $\alpha^{(R)} = 0$ the average line energy density

$$\langle E'\rangle = \frac{\rho_m}{2}\int_C dy\; dz\langle \boldsymbol{v}^2\rangle = \rho_m\nu^2 C'\left([f_x,f_x]+[f_z,f_z]\right)\langle|A|^2\rangle \tag{7.30}$$

of the fluctuations in physical units,

$$\langle E'\rangle_{RBC} = \frac{k_B T}{4d\xi_0\sqrt{|\epsilon|}(-\lambda_0\tau_0)} \tag{7.31}$$

where $\lambda_0 = \lambda(\epsilon=-1,k=k_c)$ is the equilibrium-growth rate of the mode becoming unstable at threshold and, for no-slip BC, $\xi_0 = 0.38$ and $-\lambda_0\tau_0 = 1+1.93P$. In deriving (7.31) I used (7.23), the stationary fluctuations (7.22) of the scaled 1D amplitude equation, expressed f_x in terms of f_z and used (7.29) with $I_{z\theta} := [f_z,f_z]/[f_z,f_\theta]$ given below in (7.34) and an analogous integral expression for λ_0. There is an additional

factor $e^{-|x/\xi|}\cos k_c x$ with the correlation length $\xi = \xi_0/\sqrt{-\epsilon}$ for two-point equal-time velocity correlations with separation x. For 2D and near threshold the corresponding energy per area is $k_c/2$ times the line energy density (7.31) [131].

Equation (7.31) states that in 1D the mean kinetic energy of velocity fluctuations in a volume with unscaled cross section C and twice the unscaled correlation length ξd is $\frac{1}{2}k_BT(\tau_0|\lambda_0|\epsilon)^{-1}$. In 2D the corresponding volume is d times the area $(\xi d)(4\lambda_{roll}/\pi)$ with $\lambda_{roll} = \pi/k_c$. This appears, especially for $P \to 0$ ($\lambda_0\tau_0 \to -1$), similar to equipartition-theorem fluctuations. Indeed, calculating the average energy of velocity fluctuations contained in one Fourier-mode pair with (7.19) and (7.16) gives, for arbitrary vertical BC and Prandtl numbers and periodic BC in x and y,

$$\frac{\rho_m}{2}\int_V d^3r\langle(|\boldsymbol{v}_k|^2 + |\boldsymbol{v}_{-k}|^2)\rangle = \frac{k_BT}{|\epsilon|}\begin{cases} 1 & P = 0 \text{ or } \epsilon = -1, \\ (|\lambda_0|\tau_0)^{-1} & \epsilon \to 0_-, \end{cases} \tag{7.32}$$

where V is the volume of the system. Without temperature gradient ($\epsilon = -1$) the kinetic energy contained in these fluctuations fulfills the equipartition theorem (two physical degrees of freedom per wave-vector pair). For zero Prandtl number the fluctuations increase like $-1/\epsilon$ if a temperature gradient is applied.

7.4.2 Taylor–Couette flow

The system consists of two concentric cylinders of inner and outer radii R_1 and R_2, rotating at angular frequencies Ω_1 and Ω_2, respectively. We scale lengths and time as in RBC, where d is now the gap width $R_2 - R_1$, and take as control parameter the dimensionless inner rotation $\omega_1 = \Omega_1 d^2/\nu$. The outer rotation $\omega_2 = \Omega_2 d^2/\nu$ and the radius ratio $\eta = R_1/R_2$ are fixed parameters. The system is effectively one-dimensional and described best in cylindrical coordinates $r_\parallel = z$ and $r_\perp = (r, \phi)$. In a range of the control parameters where the first instability of the basic Couette flow leads to axisymmetric vortices [9], the amplitude equation for $A(z,t)$ without through flow is the same as Eq. (7.26) for 1D-RBC. With axial through flow there is an additional group velocity term $v_g\partial_x A$ where v_g is 1.23 times the mean axial velocity of the through flow (1.05 times the phase velocity of the vortices) and furthermore the other coefficients have very small imaginary parts [132].

The only noise source in the basic equations [73] comes from the stress tensor in the Navier-Stokes equations for the deviations of the velocity from the basic Couette flow. In cylindrical coordinates one gets (the indices take the values r, ϕ, and z) $(\boldsymbol{\nabla}\underline{\underline{\sigma}})_i = D^{(vv)}_{i,jk}\sigma_{jk}$ with $D^{(vv)}_{ij,k} = (\delta_{ik}r^{-1}\partial_j r + r^{-1}\delta_{k2}(\delta_{i2}\delta_{j1} - \delta_{i1}\delta_{j2}))$. The Hermitean conjugates with respect to (7.15) are $D^{\dagger(vv)}_{jk,i} = -\delta_{ik}\partial_j + r^{-1}\delta_{k2}(\delta_{i2}\delta_{j1} - \delta_{i1}\delta_{j2})$. A straightforward calculation of Eq. (7.21) gives an expression for the noise strength of the TCF amplitude equation which is similar to (7.27). Instead of writing it down (see [121, 122]) I use the fact that for $\omega_2 > 0$ the Taylor system can be mapped onto RBC to second order in the gap width $1 - \eta$ yielding explicit analytic expressions

in terms of RBC parameters [122]. The resulting noise intensity of the amplitude equation is

$$[f_r, f_r] Q^{(T)}(\omega_2, \eta) \approx \frac{Q_0^{(R)}(1+\alpha^{(T)}) I_{z\theta}}{\pi \overline{r} \tau_0^{2(R)}|_{P=1}}, \tag{7.33}$$

where

$$I_{z\theta} = \frac{[f_z, f_z]}{[f_z, f_\theta]} = \frac{k_c^2 [f_z, f_z]}{[f_z, (k_c^2 - \partial_z^2)^2 f_z]}, \tag{7.34}$$

$$\alpha^{(T)} = \frac{4\omega^2(\overline{r})}{R_c}, \qquad \overline{r} = \frac{R_1 + R_2}{2d}. \tag{7.35}$$

The radial eigenfunction f_r corresponds to f_z in the RBC system and $\omega(\overline{r})$ denotes the squared dimensionless angular velocity of the basic Couette-flow $\omega(\overline{r})$ [73] in the middle of the gap. For no-slip BC ($R_c = 1708$, $\tau_0^{(R)} = 0.077$, $I_{z\theta} = 0.013$) the error with respect to a calculation of (7.21) using numerically obtained eigenfunctions [121] is less than 2.5% for $\eta = 0.738$ and all $\omega_2 \geq 0$ [122]. Smaller gaps (larger η) should make the approximation even better since the mapping onto RBC gets exact for $\eta \to 1$.

Eqation (7.33) states that, if one relates the amplitude to v_r in TCF and to v_z in RBC, the noise strength of the amplitude equation for axisymmetric TCF vortices is $(1+\alpha^{(T)})/(1+\alpha^{(R)}) \approx (1+\alpha^{(T)})$ times the noise strength of 1D-RBC with $P = 1$, a width $2\pi\overline{r}$, and periodic BC in y. While in RBC the relative influence $\alpha^{(R)}$ of the temperature fluctuations is negligible, the relative influence $\alpha^{(T)}$ of v_ϕ fluctuations on fluctuations of the axisymmetric Taylor vortices dominates for large corotation rates ω_2. Velocity fluctuations, integrated over the respective cross sections, should be comparable in both systems if they are at the same (small, negative) distance ϵ from threshold [133]. For the mean line energy $\langle E' \rangle_{TCF} = \frac{\rho_m}{2} \int_C r \; dr d\phi \langle v_r^2 + v_z^2 \rangle^{(T)}$, contained in the fluctuations of the velocity components v_r and v_z which correspond to v_z and v_x in RBC, one obtains

$$\langle E' \rangle_{TCF} = \frac{k_B T}{(4d\xi_0\sqrt{|\epsilon|})} \frac{(1+\alpha^{(T)})}{(-\lambda_0^{(R)}\tau_0^{(R)})} \left(\frac{\tau_0^{(T)}}{\tau_0^{(R)}} \right). \tag{7.36}$$

With $\tau_0^{(T)}/\tau_0^{(R)} = \xi_0^2/\xi_0^{2(R)}$ (Ref. [122]) the mean energy per length is effectively $(1+\alpha^{(T)})(\tau_0^{(T)}/\tau_0^{(R)})^{1/2}$ times the RBC line energy density which is $\langle E' \rangle_{RBC} = 0.225 k_B T/(d\sqrt{|\epsilon|})$ for no-slip BC.

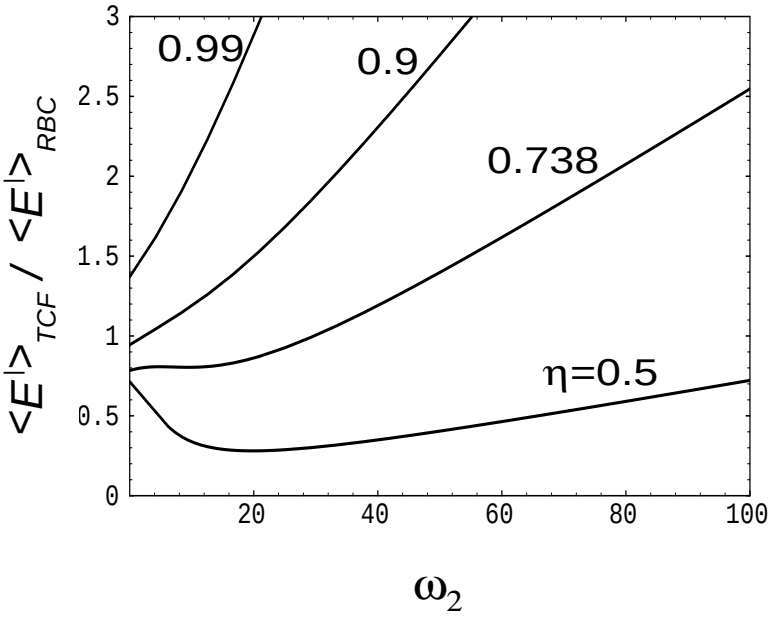

FIGURE 7.1. Average line energy contained in the fluctuations of the radial and axial velocity components of axisymmetric Taylor vortices with realistic no-slip BC. The plot shows the enhancement factor $(1+\alpha^{(T)})(\tau_0^{(T)}/\tau_0^{(R)})^{1/2}$ of the line energy density with respect to that of the equivalent one-dimensional Rayleigh–Bénard system with Prandtl number $P = 1$ and the same distance ϵ from threshold. The hoerizontal axis is the dimensionless corotation $\omega_2 = \Omega_2 d^2 \rho_m/\nu$ of the outer cylinder. Parameter is the radius ratio η.

Figure 7.1 shows a plot of this enhancement factor for various outer corotation rates ω_2 and radius ratii η. For the outer cylinder at rest ($\omega_2 = 0$) and a radius ratio $\eta = 0.738$ as in [121], the line energy is nearly the same as for RBC with $P = 1$ (factor 0.94). Without external stress ($\omega_1 = \omega_2 = \alpha^{(T)} = 0$) one recovers again equipartition-theorem results .

7.4.3 Planar electrohydrodynamic convection

The system consists of a thin liquid crystal cell (thickness d) sandwiched between two planar electrodes. The external stress is an applied AC voltage $V(t) = \sqrt{2}V_0 \cos\omega_0 t$; the control parameter is V_0^2 for fixed ω_0 and $\epsilon = V_0^2/V_c^2 - 1$. We assume planar BC $\boldsymbol{n} = (1,0,0)$ making the system anisotropic in the infinite directions and consider

a range of ω_0 and of the material parameters, where the first instability at V_c is to normal rolls $\boldsymbol{k}_c = (q_c, 0)$ (roll axis normal to equilibrium director orientation) with an essentially time independent splay-bend director mode (conductive regime) [48]. The system is quasi two dimensional. Choosing $r_{\|} = (x, y), r_{\perp} = z$, the amplitude equation (7.20) reduces to

$$\tau_0 \partial_t A(x, y, t) = (\epsilon + \xi_{0x}^2 \partial_x^2 + \xi_{0y}^2 \partial_y^2) A + \tau_0 \sqrt{Q} \eta(x, y, t). \tag{7.37}$$

The basic charge conservation, director, and nematic Navier–Stokes equations for the deviations $(\phi, \delta\boldsymbol{n}, \boldsymbol{v})$ of the basic state $(\sqrt{2} V_0 \frac{z}{d} \cos \omega_0 t, \boldsymbol{n}_0, 0)$ have periodic coefficients [48]. Stochastic forces come from the fluctuations of $\boldsymbol{j}^{(el)}$ in the charge equation (see example 2 at the end of Section 2), from the antisymmetric stress tensor $\sigma_{ij}^{(as)}$ in the director equation (example 3) and from both parts of σ_{ij} in the fluid equation (example 1). The noise correlation matrix $\underline{\underline{Q}}$ from equation (7.18), calculated with the anisotropic Onsager matrix (7.8) without the temperature components, is given in [120], Equation (67).

To calculate the threshold and the eigenfunctions in (7.21) I apply the lowest-order time-Fourier expansion for the conductive mode and lowest-order trial functions satisfying no-slip planar BC's for the z dependencies of all fields [120]. Furthermore I eliminate the velocities adiabatically. With lengths scaled by d and times by the director relaxation time $\tau_d = \gamma_1 d^2/(K_{11}\pi^2)$ (K_{11} is the splay elastic constant and γ_1 the rotational viscosity), a straightforward but lengthy calculation of (7.21) gives eventually for the parameter set of MBBA I [120],

$$[f_{n_z}, f_{n_z}]Q = \frac{2Q_0^{(E)}|\lambda_0|}{C'K} \left(\frac{1 + \alpha^{(E)}}{(\tau_0 \lambda_0)^2} + O(\frac{\omega_0}{\omega_{cutoff}})^2 \right), \tag{7.38}$$

where $|\lambda_0|/K = 1.84$, $\alpha^{(E)} = 14.9 P_1$, $|\lambda_0|\tau_0 = 1 + 9.3 P_1$ and $P_1 = \tau_{el}/\tau_d \approx 2.81(\mu m/d)^2$. The left-hand side of (7.38) is proportional to the fluctuations of n_z, a quantity which is related to the fluctuations of light modulations in the shadowgraph method, see Section 5.

The quantity $|\lambda_0|/K$ with $K = [f_{n_z}, (K_{33}q^2/K_{11} - \partial_z^2) f_{n_z}]/[f_{n_z}, f_{n_z}]$ is the ratio of the energy dissipation rate to the elastic energy of the fluctuating mode. The ratio P_1 of the time scales $\tau_{el} = \epsilon_0 \epsilon_{\perp}/\sigma_{\perp}$ and τ_d of the electric and director subsystems is the analog of the Prandtl number in RBC. The relative contribution $\alpha^{(E)}$ of the charge fluctuations is the analog of the temperature fluctuations in RBC and the v_ϕ fluctuations in TCF. Since both, $\alpha^{(E)}$ and P_1, are proportional to d^{-2}, charge fluctuations become important for thin cells. In principle there is a second time-scale ratio $d^2 \rho_m/(\nu \tau_d)$ of the time scales of the fluid and director subsystems but it turns out to be negligibly small ($\approx 10^{-6}$). This justifies the adiabatic elimination of the velocities and implies that the velocity fluctuations, which play the main role in RBC, are negligible here.

The prefactor

$$Q_0^{(E)} = \frac{k_B T}{K_{11} d} \approx 10^{-3} \frac{\mu\mathrm{m}}{d} \tag{7.39}$$

is much larger than in RBC or TCF making EHC the best candidate for quantitative fluctuation measurements.

As in the other systems one can calculate the mean line and area densities of the orientational-elastic energy contained in the fluctuations of the splay-bend director modes. Although typical EHC systems have large aspect ratios and are quasi two dimensional, the line energy density $\langle E' \rangle_{EHC} = \frac{1}{2} \int_C dy\, dz \{K_{11}(\partial_z n_z)^2 + K_{33}(\partial_x n_z)^2\} = \frac{1}{2} K_{11} K C'[f_{n_z}, f_{n_z}] \langle |A|^2 \rangle$ (proportional to the integrated director fluctuations) makes sense if interpreted as energy contained in all Fourier modes with $k_y = 0$. Indeed it is this quantity which was measured in the experiments of reference [97] as described in the next section. With the 1D version of (7.37), (7.38) and (7.22) one obtains

$$\langle E' \rangle_{EHC} = \frac{k_B T}{4 \xi_0 d \sqrt{|\epsilon|}} \beta \tag{7.40}$$

with

$$\beta = \frac{1 + \alpha^{(E)}}{|\lambda_0| \tau_0}, \tag{7.41}$$

remarkably similar to (7.31) and (7.36) although the energy itself is quite different in nature, here an elastic energy while in RBC and TCF a kinetic energy.

There is no simple expression for the energy per area in the 2D system [134]. Very near to the Lifshitz point where the correlation length ξ_{0y} vanishes [48], dimensional arguments lead to an $|\epsilon|^{-1/4}$ behavior (for the 1D case a crossover from $|\epsilon|^{-1/2}$ to $|\epsilon|^{-3/4}$ is predicted [120]).

Finally one can again compare the mean orientational-elastic energy of the critical (discrete) Fourier-mode pair with the equipartition theorem. With (7.19) and the 0D version of (7.38) for a volume $V = L_x L_y d$ and periodic BC in x and y one obtains near threshold

$$\langle E_{k_c}^{(E)} + E_{-k_c}^{(E)} \rangle = \frac{k_B T}{|\epsilon|} \beta. \tag{7.42}$$

The factor β comes from the electric degrees of freedom, both stochastic (relative influence of charge fluctuations $\propto \alpha^{(E)}$) and deterministic ($\lambda_0 \tau_0 \neq -1$ due to two comparable time scales). The relative influence $\beta - 1$ of the electric degrees of freedom onto the director fluctuations vanishes for $P_1 = 0$, i.e., if the electric variables can be adiabatically eliminated. A more general calculation for $\boldsymbol{k} \neq \boldsymbol{k}_c$ and $0 > \epsilon \geq -1$ with (7.17) shows that $\beta(\boldsymbol{k}, P_1, \epsilon \to -1) \to 1$, i.e., without external stress the equipartition-theorem result is recovered.

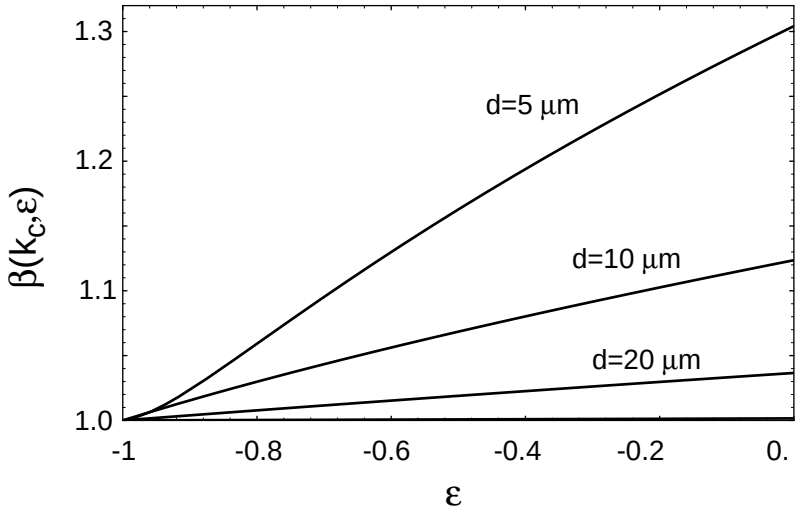

FIGURE 7.2. Influence of the electric degrees of freedom (charge fluctuations and change of the relaxation time) on director fluctuations of EHC for external frequencies much smaller than the cutoff frequency and relatively small charge relaxation times. The plot shows the enhancement factor $\beta(k_c, \epsilon)$ for the energy of the critical splay-bend Fourier mode with respect to $k_B T/(2|\epsilon|)$ which would be obtained by adiabatically eliminating the charge and neglecting charge fluctuations. The horizontal axis denotes the reduced control parameter where $\epsilon = -1$ (no external stress) corresponds to an equilibrium system. Parameter is the cell thickness $d \propto (\tau_d/\tau_q)^{1/2}$. For $\epsilon \to 0$, β is given by Eq. (7.41).

Figure 7.2 shows a plot of the enhancement factor $\beta(k_c, \epsilon)$ as a function of ϵ for some values of the cell thickness ($P_1 \propto d^{-2}$).

Note that even for negligible charge fluctuations the conductivity and thus the nonequilibrium property is essential since it influences the relaxation time. Without electric conductivity, but leaving the other MBBA parameters unchanged, the stabilizing effect of the negative dielectric anisotropy would lead to decreased instead of enhanced fluctuations for increasing V_0.

7.5 Experimental results

A common difficulty in measuring thermal fluctuations in pattern-forming system is their small magnitude, expressed by the prefactors $Q_0^{(R)}$ and $Q_0^{(E)}$. To measure the fluctuations directly, one needs a system with a favourable Q_0 and as little imperfections as possible, to be able to go very near threshold.

Both $Q_0^{(R)}$ and $Q_0^{(E)}$ can be increased by decreasing the thickness and $Q_0^{(R)}$ also by decreasing ρ_m making gasses (ν comparable with fluids) the favourable RBC system. A lower limit for the thickness in RBC is set by the temperature difference $\propto \nu/d^3$ needed to reach the threshold together with the requirement that there is no freezing at the top and boiling at the bottom. In EHC the critical voltage of the conductive mode is independent of the thickness (at least as long as the ratio of the charge relaxation time to the director relaxation time, $P_1 \propto d^{-2}$, is much smaller than unity [48]) and the limiting factor for d is electric breakthrough. In addition, for small d the director relaxation time becomes comparable with τ_q, a regime which is not yet investigated systematically.

In general the conditions for EHC are more favourable than in the RB systems. So up to very recently EHC was the only system where thermal fluctuations could be measured directly [97, 135, 113]. In reference [97] director fluctuations of a thin ($d = 13$ μm) cell of MBBA with an aspect ratio of about 1000 (quasi-2D) were determined with the shadowgraph method [39], i.e., by measuring intensity modulations of transmitted light. This method uses the dependence of the refractive index on the director orientation. For small fluctuations around the equilibrium alignment $\boldsymbol{n}_0 = (1,0,0)$, the light modulations $\tilde{I}(x,y,t) = I(x,y,t)/I_0 - 1$ are proportional to the z integrated director bend, $\tilde{I} = -\delta_{EHC}\partial_x \overline{n}_z$ with $\overline{n}_z(x,y,t) = \int dz n_z(\boldsymbol{r},t)$ and known shadowgraph sensitivity δ_{EHC} [39, 136]. If one normalizes f_{n_z} to $\int dz f_{n_z} = 1$, the theoretically calculated structure function $S(\Delta x, \Delta y, \Delta t) := \langle \tilde{I}(x+\Delta x, y+\Delta y, t+\Delta t)\tilde{I}(x,y,t)\rangle$ is related to the correlations of the amplitude fluctuations in the case of stationary normal rolls by

$$\begin{aligned} S(\Delta x, \Delta y, \Delta t) &= 2q_c^2\delta_{EHC}^2 \langle A^*(x,y,t)A(x+\Delta x, y+\Delta y, t+\Delta t)\rangle \\ &\quad \cos q_c \Delta x. \end{aligned} \tag{7.43}$$

The photodetector integrated in y over a length $L_y = 13.4d$, which is larger than the actual correlation length in y for typical ϵ values. So it measured in this direction effectively the discrete Fourier component at $k_y = 0$, $\tilde{I}(x,t) = L_y^{-1}\int_0^{L_y} dy\ \tilde{I}(x,y,t)$. The measured 1D-correlations $S(\Delta x, \Delta t)$ should correspond to the amplitude correlations of an 1D system with cross-section dL_y and periodic BC in y, i.e., effectively to the 1D version of (7.37) with $\partial_y = 0$ and a noise strength $Q_{1D}^{(E)} = L_y^{-1}Q_{2D}^{(E)}$.

Recall that all considerations about fluctuations in EHC in this chapter are based onto the SM. In the above system, however, one observes travelling waves above threshold and consistent with this, the observed fluctuations oscillate in time, see

Fig.4 of [97]. For all time delays the correlations were reflection symmetric in x showing that they are caused by fluctuations of right and left travelling waves in statistically equal proportions indicating a Hopf bifurcation [137].

In the simplest case this can be captured by assuming for the two waves $(\pm\omega_c, k_c, 0)$ two independent 1D-stochastic amplitude equations of the form (7.37) with group-velocity terms $\pm v_g \partial_x A$ added on their left-hand sides. The structure function then has two contributions of the form (7.43) with $\cos q_c \Delta x$ replaced by $\cos(q_c \Delta x \mp \omega_c \Delta t)$. Analytically calculated correlations of the amplitude equations [97] lead to a structure function which agrees, as function of space and time delay, very well with the measured one.

The structure function shows the predicted symmetries and the increase of fluctuation intensity and correlation lengths and times, as one approaches the threshold. The equal-time correlations (7.22) for each of the waves, $< A^*(x,t)A(x+\Delta x,t) > = \langle |A|^2 \rangle e^{-\xi|\Delta x|}$ with $\langle |A|^2 \rangle = Q/(8\tau_0 \xi_0 \sqrt{|\epsilon|})$ have the predicted correlation length $\xi = \xi_0 |\epsilon|^{-1/2}$ and an intensity $\propto |\epsilon|^{-1/2}$ consistent with the measured equal-time structure function $S(\Delta x,\, \Delta t = 0)$. The decay of $S(\Delta x = 0, \Delta t)$ with time delay is also in good agreement with the prediction. The oscillations of S have about the same wavelength and frequency as the deterministic pattern above threshold. In addition the *absolute* fluctuation intensity agrees within a factor of about 1.3 with the theoretical prediction (7.40). The measured intensity corresponds to $\beta_{exp} \approx 1.44$ while the theoretical prediction (7.41) can be taken from Fig. 7.2 yielding $\beta = 1.1$ for $d = 13\mu$m and $\epsilon = 0$.

Similar good agreement is found in [135] by measuring the shadowgraph signal in a MBBA cell with 23μm thickness. In agreement with (7.42) both the correlation time and the intensity as obtained from the Fourier-mode pair with the critical wave vector are $\propto |\epsilon|^{-1}$. The measured absolute intensity, $\beta_{exp} = 1.3$, was 30% above equipartition-theorem estimates while the theory predicts $\beta = 1.03$.

Hörner et al [113] have measured spatial correlations of fluctuations in a cell filled with the nematic Merck Phase V. For low external frequencies this material has a (deterministic) bifurcation to oblique rolls, i.e., a degenerated bifurcation to zig and zag rolls.

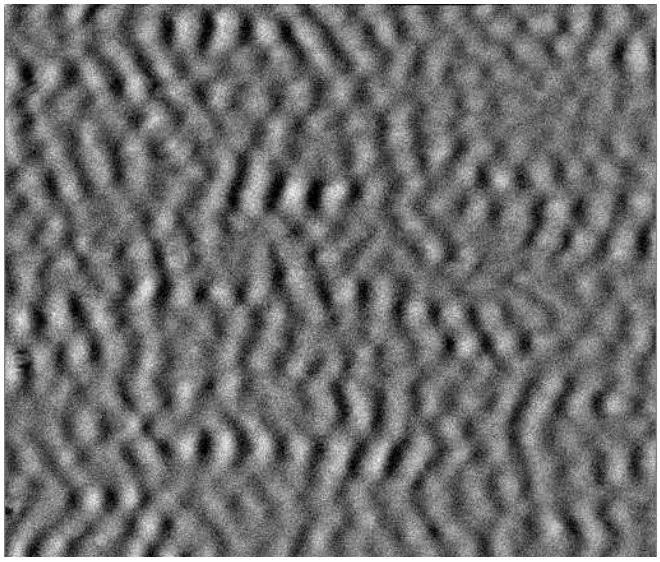

FIGURE 7.3. Shadowgraph image of subctritical fluctuations near the threshold of electroconvection of the nematic Merck Phase V in a frequency regime where there would be oblique rolls above threshold. (Courtesy of I. Rehberg and F. Hörner).

Figure 7.3 shows a snapshot of the resulting shadowgraph intensity. According to theory the equal-time structure function (spatial correlation) has now two contributions of the form (7.43) with $\cos q_c \Delta x$ replaced by $\cos(q_c \Delta x \pm p_c \Delta y)$ and the amplitude equation has the general form (7.20) with real coefficients and $v_g = 0$. The spatial Fourier transform of the theoretically calculated structure function, $S(k_x, k_y)$, has four peaks at the wave vectors $\pm \boldsymbol{k}_{zig}$ and $\pm \boldsymbol{k}_{zag}$. The structure function obtained from Fig. 7.3 shows qualitative agreement with the theoretical prediction.

Recently, fluctuations were measured directly in effectively two-dimensional RBC in gaseous CO_2 at elevated pressures [131] and in an effectively one-dimensional convection channel in a binary mixture of ethanol and water [138]. In the CO_2 experiment, $Q_0^{(R)}$ is larger than in liquids but nevertheless the measured signal required extensive processing. As in the EHC experiments, the fluctuations were measured with the shadowgraph technique. Here the refractive index depends on the density and on the temperature *via* the expansion coefficient. The shadowgraph signal for light, incident in the z direction, is $\tilde{I}(x, y, t) = -\delta_{RBC} \nabla_\perp^2 \overline{\theta}$ with $\overline{\theta} = \int dz \theta$ and known sensitivity δ_{RBC}[131]. Near threshold the relevant contributions to the fluctuating

pattern include all wave vectors with $|k| \approx k_c$. With f_θ normalized to $\int dz f_\theta = 1$, the modulation amplitude $\tilde{I} = \delta_{RBC} k_c^2 \psi$ is directly proportional to the amplitude of the stochastic Swift–Hohenberg equation and the theoretically determined structure function $S(\Delta x, \Delta y, \Delta t) = \delta_{RBC}^2 k_c^4 \langle \psi^* \psi \rangle$ is given by the amplitude correlations. The measured spatial Fourier transform of the equal-time structure function agreed well with the theoretical prediction near threshold, $S(\boldsymbol{k}) = S_0/((k - k_c)^2 + |\epsilon|)$ [131] with $S_0 = \delta_{RBC}^2 k_c^4 Q \tau_0/(2(2\pi)^2)$ from Eq. (7.19). In particular it is isotropic, large in a ring of radius k_c and the peak at k_c is proportional to $|\epsilon|^{-1}$. In real space, both the absolute intensity of the temperature fluctuations and the $|\epsilon|^{-1/2}$ behavior agreed perfectly with the theoretical prediction $\propto \int d^2 k S(\boldsymbol{k})$ for high pressures where the Boussinesq approximation holds. For lower pressures the experimental values were up to 20% *smaller*.

In the experiment on binary mixtures [138], the fluctuations are observed in a parameter regime where the first instability is a Hopf bifurcation leading to travelling waves because these time–dependent patterns can be observed with a better signal–to–noise ratio than stationary ones. The fluctuation intensity shows the correct $|\epsilon|^{-1/2}$ behavior of 1D systems and the magnitude is of the same order as idealized theoretical estimates.

So far I described direct measurements. A possibility to overcome the difficulties with the small signal are indirect measurements where the fluctuations are enhanced by some amplifying mechanism prior to measurement.

The amplification mechanism can be external by applying control–parameter ramps in time going from sub- to supercritical values. As soon as the control parameter is supercritical, the small, initially subcritical, fluctuations grow exponentially until they become measurable. Measurements on RBC with this method gave the first experimental evidence of stochastic effects in pattern–forming systems [139, 140]. As in the direct measurements, the structure factor in Fourier space had a maximum along a ring with radius k_c. The intensity, however, was about a factor of 2×10^4 larger than predicted for thermal fluctuations.

Another possibility is internal amplification in space in the convectively unstable regime in systems with a nonzero group velocity [123]. Above the convective instability fluctuations are amplified as they travel through the system. If one is also above the absolute threshold, they would grow in the whole system to nonlinear saturation and eventually the system would reach a deterministic attractor. Below the absolute threshold, however, the propagation velocity of perturbations, determined by the growth rate and the spreading by diffusion, is smaller than the group velocity so that fluctuations are convected away faster than they can grow. So at least in parts of the system the fluctuations are both linear and much larger than the subcritical ones, and the resulting "noise–sustained structures" [132] can be measured. Typically systems with nonzero group velocity have a Hopf bifurcation or are open

systems, e.g., RBC or TCF with throughflow.

The Hopf bifurcation of RBC in binary–fluid mixtures with a negative separation ratio [9] was used to measure fluctuations in an quasi–1D cell [141, 138]. Theoretically this system is described by two stochastic 1D complex amplitude equations similar to the ones used in EHC above. The dissipative effect of mass diffusion leads (compare Eqs. (7.21) and (7.18)) to an additional term in the RBC fluctuation strength (7.27) which has been calculated in [119] and was found to be small [142]. The interpretation is difficult because the fluctuations described by these stochastic equations depend strongly on the boundary conditions which in the experiment correspond to ramps consisting of decreasing height on both sides of the cell. Analytic calculations with an effective cell length [141] lead to a fluctuation intensity in accordance with the experiment whereas numerical calculations taking into account more realistic BC by introducing a space dependent control parameter at each side lead to fluctuation intensities about two orders of magnitude smaller than the measured ones [143]. A possible explanation of this large discrepancy is the exponential dependence of the intensity on the assumed effective cell length in the analytic calculation together with the fact that there is no obvious way to define this length.

Things are easier to interprete in open–flow systems where there is only one travelling wave and the downstream BC is irrelevant (in the convectively unstable regime information cannot travel upwards). Numerical simulations showed that the fluctuations are even rather insensitive to the upstream BC. Even if one sets the upstream fluctuations at the inlet equal to zero, the stochastic volume force would create fluctuations which after a short distance from the inlet are nearly the same as with more realistic equilibrium fluctuations at the inlet [121]. In any case the fluctuations are amplified on their way through the system until they become measurable and eventually saturate at the "healing length". In a way the experiments in open–flow systems are the analog in space to the ramping experiments in time. In the former, time is translated to space by the group velocity. Measurements of the rms value of axial velocity fluctuations in TCF with through flow with a laser–Doppler interferometer [121] agreed with theory in all aspects except the absolute fluctuation intensity which was by a factor of 270 larger than the predicted value $\nu^2/d^2 \times [f_z, f_z] Q^{(T)} \tau_0 / (4\xi_0 \sqrt{-\epsilon})$ for thermal fluctuations.

7.6 Discussion

In this chapter I tried to provide an understanding of fluctuations near pattern–forming transitions in nonequilibrium extended systems starting from stochastic hydrodynamics, an approach formulated by Landau [68] to describe equilibrium hydrodynamic fluctuations in simple fluids. The *rationale* to extend this approach to nonequilibrium systems is that it requires only local equilibrium which is fulfilled

in many hydrodynamic systems which are far from global equilibrium. In addition the separation of scales between the microscopic and macroscopic degrees of freedom justifies the assumption that the fluctuating forces are δ correlated.

Fluctuating hydrodynamics makes definite predictions about the fluctuations as a function of the quasi–dimensionality and the distance from threshold. The correlation functions of the fluctuations oscillate as function of space and time separation with about the same period as the deterministic pattern and below threshold they retain all symmetries of the system. Correlation lengths and times, and the fluctuation intensity, increase with the proximity to the deterministic threshold, with scaling exponents which depend on the symmetries and the quasi–dimensionality. This means that the fluctuations in real space consist of patches with the size of about the correlation length, living for about one correlation time. Each patch is a wave packet of one degenerate mode out of the uniformly distributed set of critical modes. The fluctuations anticipate, in a way, the possible deterministic patterns above the primary threshold.

In 1D systems, many of these features are analogous to equilibrium fluctuations. The scaling exponents of correlation lengths, times and of the intensity are the same. In 2D, pattern–forming systems with continous degeneracy (RBC or EHC at the transition from normal to oblique rolls) offer new and fascinating symmetry classes of transitions. If only one field is dynamically active (e.g., n_z for normal rolls in EHC with $P_1 \to 0$ or v_z for RBC with $P \to 0$), the average energy contained in the fluctuations of one Fourier mode or, equivalently, the energy in a fluid element of half the size of the correlation length in 1D systems, is $|\epsilon|^{-1}$ times the equipartition–theorem fluctuations $k_BT/2$. This is again as in equilibrium, for example below the splay–bend Fréedericksz transition in planar EHC. Additional dynamically active fields lead both to new fluctuating forces summarized in the terms proportional to $\alpha^{(R)}$, $\alpha^{(T)}$ and $\alpha^{(E)}$ in Eqs. (7.29), (7.36) and (7.40) with (7.41), and to a deterministic influence on the relaxation rate, making $(-\lambda_0\tau_0)$ unequal to unity, from Sec. 4 $(-\lambda_0\tau_0) = 1 + 1.93P$ in RBC, $2.93\tau_0^{(T)}/\tau_0^{(R)}$ in TCF and $1 + 9.3\tau_{el}/\tau_d$ in EHC. The net effect on the fluctuations can be increasing as in the case of charge fluctuations in EHC, decreasing as for the temperature field in RBC, or dependent on a second control parameter as in TCF.

The above predictions agree with experiments. One sees patches of zig and zag rolls in the oblique–roll regime of EHC, areas of left and right travelling waves if there is a Hopf bifurcation, and isotropically distributed roll directions in RBC in simple fluids corresponding to a ring in k space.

The above features are predicted for *any* noise source if its correlations in space and time are much smaller than the macroscopic scales. To show that *thermal* fluctuations are involved and that stochastic hydrodynamics provides the correct thermodynamical description of nonequilibrium systems near a phase transition, the

absolute value of the fluctuation intensity must agree with the experiment. This is the case in the direct measurements of the EHC and RBC systems described above. [The fact that the measured fluctuations in the RBC experiments are up to 20% smaller for low pressures, can probably be explained by using the non–Boussinesq equations in Eqs. (7.21) and (7.18).]

An open question is the observed fluctuation intensity in the indirect experiments. In the open-flow experiment [132], the observed fluctuation intensity is more than two orders of magnitude too large; in the time-ramping experiments [139, 140] the discrepancy is even four orders of magnitude, and in the binary-mixture experiment using travelling waves as amplification mechanism [141] it is difficult to interpret. An investigation primarily aimed at describing nonlinear transient patterns in the splay Fréedericksz transition of NLCs with positive dielectric anoisotropy [144] shows that in a situation similar to the above indirect measurements (jump of the control parameter to above threshold) even in nematics the experimental noise strength is much larger than that of thermal noise. Specifically the initial (subcritical) amplitude of the homogeneous mode obtained from the experimental fit to the nematodynamic equations is about two orders of magnitude larger than predicted by Eq. (7.42). This is strikingly similar to the time-ramping experiments [139, 140] (the intensity is equal to the square of the amplitude).

All this seems to indicate that the assumption of stochastic hydrodynamics together with local equilibrium is valid only in stationary situations. However, one has to be aware that in all indirect experiments the logarithm of the noise strength rather than the noise strength itself is measured. In the time-ramping experiments, errors in determining the effective time difference from the initial subcritical fluctuations to saturation contribute exponentially. The same is true for the effective travelling length to saturation ("healing length" l_h) in the open-flow and travelling-wave experiments and, in all three indirect experiments, for the uncertainty in the distance from the convective threshold. We take as an example the TCF experiment [132] in the regime of convective instability $0 < \epsilon \leq \epsilon_a$. The fluctuation intensity is roughly $e^{2\beta z}$ times the fluctuations at the inlet $z = 0$ where the spatial growth rate β increases monotonically with ϵ and is essentially proportional to ϵ if one is not too close to the absolute threshold [121]. If one assumes at the inlet *a priori* thermal equilibrium fluctuations $\langle \overline{\theta}^2 \rangle = \gamma Q$ with known constant γ (and not larger inlet fluctuations due to additional experimental noise), the intensity at the nonlinear saturation for typical threshold distances is about nine orders of magnitude larger. The fluctuations were measured only in the region where the intensity is more than 0.01 times the saturation value, so, experimentally, the strength of the fluctuating forces is essentially inferred from the healing length l_h by $\gamma Q_{exp} = \langle \overline{\theta}^2 (z = 0) \rangle = e^{-2\beta l_h} \langle \overline{\theta}^2 \rangle_{sat}$. With known saturation fluctuations and assuming $\beta \propto \epsilon$, the error in the decadic logarithm of the experimental noise strength, $\Delta(\log_{10} Q_{exp})$, is $9(\Delta\epsilon/\epsilon)$ and $9(\Delta l_h/l_h)$ due to the relative errors in the threshold distance and the healing length, respectively.

A relative error of 0.22 in one of these quantities would lead to a factor of 100 in the measured noise strength. Note that β depends also on other parameters of the amplitude equation like τ_0 and ξ_0 [121], whose errors contribute similarly.